Soft Matter

PAPER

View Article Online
View Journal | View Issue

Cite this: *Soft Matter*, 2024, **20**, 6390

Lipid/polyelectrolyte complexes – effects of the polyelectrolyte architecture on the self-assembled structures†

Miriam Simon, ‡[a] Lauren Matthews §[b] and Yeshayahu Talmon *[a]

Self-assembly is a key process in forming biological materials. Especially the interaction between amphiphiles and polyelectrolytes has been widely investigated in recent years due to their potential application in industry and medicine, with a special focus on gene therapy. Accordingly, we investigated the formation of lipoplexes by mixing the cationic lipid **DOTAP** (1,2-dioleoyl-3-trimethylammonium-propane (chloride salt)) with different anionic polyelectrolytes (PE), such as **NaPA** (sodium polyacrylate), **CMC** (sodium carboxymethyl cellulose) with different degrees of substitution (DS, namely, different charge density), **PSS** (sodium polystyrenesulfonate) and **DNA** (deoxyribonucleic acid sodium salt). The goal of this project was to explore the influence of different system parameters, such as the charge ratio, CR = [+]/[−] = [**DOTAP**]/[PE], the charge density of the PE, or the type of PE on the morphology of the formed complexes. The investigation of these systems was performed by cryo-transmission electron microscopy (cryo-TEM), and with small-angle X-ray scattering (SAXS), to support our findings. In our experiments, we obtained a comprehensive picture of the formed lipoplexes, and how their structure depends on the different properties of the employed polyelectrolyte. Although the basic nanostructure of all complexes is lamellar, their detailed morphology depends strongly on parameters of the PE, *e.g.*, the persistence length, charge density, or the polymer backbone. Understanding these specific interactions will allow the formation of more stable and optimized complexes as they are needed for drug or genetic material delivery.

Received 25th April 2024,
Accepted 24th July 2024

DOI: 10.1039/d4sm00489b

rsc.li/soft-matter-journal

Introduction

Self-assembly is the spontaneous and thermodynamically driven organization of molecules into multimolecular structures and a key process in forming biological materials. The formation of aggregates with different morphologies (spherical, thread-like, lamellar, *etc.*) depends on the molecular geometry, as described by the packing parameter.[1] For example, double-tailed amphiphiles, such as lipids, tend to self-assemble into lamellar structures or vesicles. These vesicles can be subdivided into different classes of multi-lamellar vesicles (MLV), large unilamellar vesicles (LUV), or small unilamellar vesicles (SUV).[2] Vesicles that mainly consist of (phospho-)lipid bilayers, are often called liposomes. Due to this phospholipid membrane, liposomes may be used as simplified model systems for biological membranes or cells. They are typically made from natural, biodegradable, nontoxic, and nonimmunogenic lipid molecules, and easily fuse with cells, and, therefore, are a promising tool for medical applications, such as drug delivery systems.[3,4]

Liposomes are widely used as delivery systems in cosmetics, such as sunscreen, creams, or hair products. For example, it was found, that the use of liposomal cream significantly contributed to repairing the surface lipid layer of the skin.[5] In the food industry, liposomes may be used to encapsulate proteins, enzymes, vitamins, or flavors.[6] Of course, liposomes are also a favored tool for drug delivery applications, as they can encapsulate hydrophilic drugs or bind hydrophobic drugs into or onto their membrane. Besides being carrier vehicles, liposomes also offer more advantages, such as protection of sensitive drug molecules and enhanced cellular uptake. New liposomal vaccines are also being developed. Here, the liposomes can act as an adjuvant, as well as a carrier for antigens and coadjuvants.[7]

[a] *Dept. of Chemical Engineering and The Russell Berrie Nanotechnology Institute (RBNI), Technion-Israel Institute of Technology, Haifa 3200003, Israel. E-mail: ishi@technion.ac.il*
[b] *ESRF, The European Synchrotron, 71 avenue des Martyrs, CS 40220, 38043 Grenoble Cedex 9, France*

† Electronic supplementary information (ESI) available. See DOI: 10.1039/d4sm00489b

‡ Present address: Bausch+Lomb GmbH, Brunsbüttler Damm 165/173, 13581 Berlin, Germany.

§ Present address: ISIS Pulsed Muon and Neutron Source, Rutherford Appleton Laboratory, Chilton, OX11 7QY, UK.

For most applications, the lipids are mixed with other compounds to modify their properties with respect to rheology, liposome size, stability, zeta potential, or phase transition temperature.[8,9] Here, especially the interactions between charged lipids and oppositely charged polyelectrolytes have been widely investigated in recent years, experimentally as well as theoretically,[10] due to their many applications in industry and medicine, with a special focus on gene therapy.

One important potential application of lipid/polyelectrolyte complexes is in transfection.[11] Transfection is the process of delivering genetic material into the cell nucleus to modify its genetic makeup. It is used as a therapy for cancer and a range of other genetic diseases. This approach is based on the complexation of **DNA** (deoxyribonucleic acid) with cationic lipids.[12,13]

Previous studies show that the addition of **DNA** to unilamellar, oppositely charged liposomes, induces disintegration of the liposomes and the formation of large multilamellar nanostructures instead, in which the polymer is sandwiched between two adjacent lipid bilayers. Alternatively, the **DNA** can be coated by lipid monolayers in an inverse hexagonal lattice.[14,15] This was shown to occur for different lipids, such as **DOTAP** (1,2-dioleoyl-3-trimethylammonium-propane (chloride salt)), DOPC (dioleoylphosphatidylcholine), BFDMA (bis(*n*-ferrocenylundecyl) dimethylammonium bromide) and others, and was studied by small-angle X-ray scattering (SAXS), dynamic light scattering (DLS), cryo-TEM.[16–18] Depending on the packing parameter of the lipid, also hexagonal structures in which thread-like lipid micelles are coated with **DNA** are possible as shown by Ewert *et al.*[19]

Lipids are available in many different forms and shapes. BFDMA, for example, contains a ferrocene group, whose oxidation state changes the net charge of the lipid. Using reduced BFDMA leads to multilamellar complexes, while aggregates with oxidized BFDMA are loose and disordered.[20] Similarly, the mixing of two lipids, *e.g.*, a charged and a neutral one, affects the structure of the formed complexes.[21] Lamellar packing of lipid molecules was typical for the complexes formed from the cationic lipid-enriched mixtures, while inverted hexagonal arrays were found for the neutral lipid-enriched complexes.

Another very important parameter, influencing the transfection efficiency, is the cationic lipid/**DNA** ratio (charge ratio). However, the influence of the charge ratio on the complex formation seems to be very specific to the materials used.[22,23]

When charged lipids are mixed with other, oppositely charged polyelectrolytes, similar structures to the complexes with **DNA** are found, but their detailed morphology depends strongly on the respective system. Many factors, such as the type of lipid, the type of polyelectrolyte, and their mixing ratio are important. Also, external stimuli, such as the pH or temperature, can influence the aggregation behavior and with this the appearance of the resulting complexes. Some examples are summarized in the next few paragraphs:

Golan *et al.* employed sodium polyacrylate, (**NaPA**) as a polyelectrolyte with two different lipids (**DOTAP** and BFDMA) and found onion-like structures, very similar to the ones previously found when mixing the same lipids with **DNA**. They suggested, that the multilamellar aggregation is energetically favorable, and may be the preferred mode of aggregation for many of those systems.[24]

The effect of polyelectrolyte stiffness was also explored previously by adding the two very different polyelectrolytes, PAA and **PSS** (polystyrene sulfonate) to **DOTAP** and DDAB (didodecyldimethyl-ammonium bromide) systems. In all systems, multilamellar nanostructures were formed, but depending on the persistence length of the polyelectrolyte, very different spacings between the lamellae were found. The molecular weight (M_w) of the polyelectrolyte did not have a marked effect.[25]

Also, external stimuli were found to influence the lipid/polyelectrolyte complexes. Many polyelectrolytes are weak acids or bases, thus the pH of the solution affects their charge density, and, through it, their interaction potential. This is known for surfactant/polyelectrolyte systems,[26] but has also been studied in lipid/polyelectrolyte complexes. If the pH is lowered below the pK_a of the polyelectrolyte, no complexes are formed.[25] Neumann, *et al.* showed how the lamellar structure of lipid/**DNA** films was sensitive to hydration and temperature.[27]

Obviously, the nanostructures of the complexes formed by lipids and polyelectrolytes also affect their macroscopic properties, be it rheological properties or the effectiveness of transfection. With respect to transfection, the scope of promising complexes for this application is not restricted to lipoplexes but can be extended to polyelectrolyte-**DNA** complexes, so-called polyplexes.[28] Recently Rappoport *et al.* studied the complexation of a double hydrophilic block-copolymer with **DNA** and found a variety of very stable structures. At the right charge ratio, hexagonal structures can be formed (preferred for transfection), which are not affected by the interaction with blood proteins for several days.[29]

In our work we are interested in finding correlations of how the molecular constitution of a system affects its self-aggregation behavior in the liquid phase, and in how the formed aggregates lead to certain properties of the system and its functions. In the present study, we investigated the interactions of liposomes with selected polyelectrolytes. The cationic lipid **DOTAP** was mixed with different anionic polyelectrolytes (PEs), such as **NaPA**, **CMC** (sodium carboxymethyl cellulose) with different degrees of substitution (DS), namely, different charge density, **PSS**, and **DNA**. The goal of this project was to explore the influence of different system parameters, such as the charge ratio CR = [+]/[−] = [**DOTAP**]/[PE], the charge density of the PE or the type of PE on the morphology of the formed complexes. We studied these systems by cryo-transmission electron microscopy (cryo-TEM), complemented by small-angle X-ray scattering (SAXS) measurements.

From our experiments, we obtained a comprehensive picture of the formed complexes, and how their detailed structure depends on the different properties of the polyelectrolytes used. Although the basic nanostructures of the complexes are lamellar, their detailed morphology depends strongly on parameters like the persistence length, charge density, or polymer backbone diameter. These aggregates serve as a model system for lipoplexes as they might be used in gene therapy systems,

where stable complexes with tunable properties are needed for optimized delivery.

Experimental

Materials

The cationic lipid **DOTAP** (1,2-dioleoyl-3-trimethylammonium-propane (chloride salt)) was purchased from Avanti Polar Lipids as a powder. As anionic polyelectrolytes, we used **NaPA** (sodium polyacrylate, average M_W ~15 kg mol^{-1}), **CMC** (sodium carboxymethyl cellulose, average M_W ~250 kg mol^{-1}) with different degrees of substitution (DS = 0.7, 0.9, and 1.2), **PSS** (sodium polystyrene sulfonate, average M_W ~70 kg mol^{-1}), and **DNA** (deoxyribonucleic acid sodium salt from salmon testes, average of 2000 base pairs[30]). All were purchased from Sigma-Aldrich, either as a 35 or 30 wt% aqueous solutions (**NaPA** and **PSS**), or as powder (all others), and used without further purification. The chemical structures are shown in Fig. 1.

Sample preparation

DOTAP liposomes were prepared by the dry film method. For this, **DOTAP** was first dissolved in chloroform and then dried with a N_2 stream and in a desiccator overnight. To prepare the liposomes, the formed dried film was dispersed in deionized water (c = 2 mM) and mixed with a tip sonicator (VibraCell VCX750, Sonics & Materials Inc., Newtown, CT; pulse: 8 s/2 s, amplitude: 35%) for ~2 min until the originally turbid solution became clear. The different polyelectrolytes were each dissolved in deionized water and diluted to reach stock solutions with a charge concentration of 4 mM.

To prepare mixed complexes, the **DOTAP** and polyelectrolyte stock solutions were mixed and diluted with water to obtain different charge ratios (CR = [+]/[−] = [**DOTAP**]/[PE]) at a constant **DOTAP** concentration of 1 mM (first **DOTAP**, then water was added, and last the PE). The complexed samples turned milky/turbid and sometimes phase-separated, showing a white precipitate settling at the bottom of the vial. The phase behavior was documented by photographs. For phase separated samples, only the supernatant was used for SAXS measurements and cryo-TEM imaging.

From previous studies, we know that the natural pH of the aqueous solutions we worked with in this study is around 7.[25] Because the pK_a of all the components in this study are well below 5, we did not control the pH of our solutions.

Methods

Cryo-TEM

Cryo-TEM specimens were prepared one day after the solutions had been mixed, on perforated carbon film grids (Ted Pella Inc., USA). The grids were plasma-etched in a PELCO EasiGlow glow-discharger (Ted Pella Inc., Redding, CA) to increase their hydrophilicity. Specimens were then prepared in a controlled environment vitrification system (CEVS) at 25 °C and 100% relative humidity.[31,32]

We imaged the specimens by an FEI (now Thermo Fisher Scientific) Talos F200C, FEG-equipped high-resolution TEM, operated at 200 kV. Specimens were equilibrated in the microscope below −178 °C in a Gatan 626 (Gatan, Pleasanton, CA) cryo-holder, and imaged using a low-dose imaging procedure to minimize electron-beam radiation-damage.[33] Contrast was enhanced by a Volta phase plate. Images were recorded digitally by an FEI Falcon III, direct-imaging camera, and afterwards processed by the Photoshop software to enhance contrast.

SAXS

Small-angle X-ray scattering (SAXS) measurements were performed on the TRUSAXS beamline, ID02 at the ESRF (Grenoble, France).[34] Measurements were carried out at 25 °C in a flow-through cell, with a ∅ = 2 mm quartz capillary. The X-ray energy was 12.23 keV (0.101 nm), and two sample-to-detector distances of 1 and 10 m were used, giving a q-range of 0.0045–7.4 nm^{-1}, where q is the magnitude of the scattering vector. 2D SAXS patterns were collected using an Eiger2 4 M pixel array detector (Dectris), and the sample transmission was measured simultaneously. The 2D patterns were normalized to an absolute intensity scale, and then, azimuthally averaged to obtain the 1D SAXS profiles. A MilliQ water background was subtracted from the data, and the corresponding datasets were merged over the two configurations.

Results and discussion

This work aims to understand how the charge ratio between cationic lipids and anionic polyelectrolytes and the charge

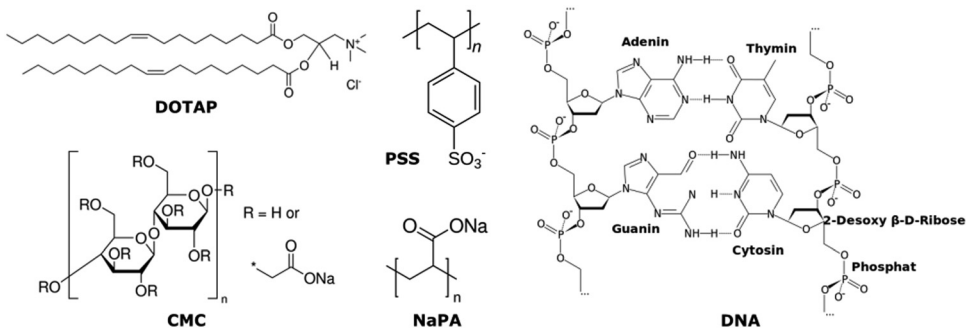

Fig. 1 Chemical structures of the lipid **DOTAP** (1,2-dioleoyl-3-trimethylammonium-propane (chloride salt)) and the four anionic polyelectrolytes **PSS** (sodium polystyrene sulfonate), **NaPA** (sodium poly-acrylate), **CMC** (sodium carboxymethyl cellulose, with different degrees of substitution (DS)) and **DNA** (deoxyribonucleic acid sodium salt).

density, the morphology, and the type of the polyelectrolyte affect the final structure of lipoplexes. First, we discuss the reference **DOTAP** samples, before mixtures of **DOTAP** and **CMC** are presented. We studied **CMC** of different charge densities, therefore the effect of charge density on the lipoplex structure can be demonstrated. Finally, we compare complexes formed with polymers of different architectures.

Pure DOTAP

As a reference sample, the pure **DOTAP** stock solution (2 mM) was examined. Cryo-TEM showed unilamellar liposomes with diameters ranging from 10 to 300 nm, see Fig. S1 (ESI†). The average membrane thickness of these liposomes as determined from the cryo-TEM images is 3.7 nm, corresponding well to the 3.72 nm **DOTAP** double layer thickness, determined by X-ray diffraction.[35] The existence of liposomes was confirmed by SAXS measurements (Fig. S2, ESI†). The increase of the intensity at the mid-q range follows a power law of q^{-2}, which can be interpreted as flat sheets, typical for vesicles. At low q, monodisperse vesicles would show oscillations, which are smeared out here, due to the wide size distribution in this sample.

Effect of charge ratio

The mixing of the positively charged **DOTAP** liposomes with a negatively charged polyelectrolyte leads to the disintegration of the liposomes and formation of large, multi-layered lipid/PE complexes, as was observed before,[25,36] and also reproduced in this work. In this study, we explored further the effect of different system parameters on the complex formation, in order to deduce correlations between polyelectrolyte characteristics and its interaction with liposomes. The visual appearance of different mixed samples already shows that small changes in the sample composition may result in very different aggregation behavior. One parameter that can be easily tuned, and was therefore the first parameter explored, is the mixing ratio of **DOTAP** and a given polyelectrolyte, *i.e.*, the charge ratio CR = [+]/[−] = [**DOTAP**]/[PE].

We studied a series of **DOTAP** liposomes mixed with the biopolyelectrolyte **CMC**1.2 (M_W = 250 kg mol^{-1}, degree of substitution, DS = 1.2) in a wide range of charge ratios, both at polyelectrolyte and at lipid excess, using visual inspection, cryo-TEM, and SAXS. When **DOTAP** and **CMC**1.2 stock solutions are mixed, a precipitation in form of a white powder can be observed (see Fig. 2). The amount of precipitated material is highest close to the charge equilibrium, at CR = 1 and 0.5, and decreases in both directions of polyelectrolyte and **DOTAP** excess. The appearance of precipitation in such systems of oppositely charged materials at a charge ratio of 1 is not unusual, and can even be expected, as here the positive and negative charges completely neutralize each other, forming uncharged complexes, which lack the electrostatic repulsion needed for stabilization. It is however surprising to see precipitation occurring even at very low charge ratios (polyelectrolyte excess), which indicates a very strong interaction between the two materials, giving precipitate of charge ratio of 1, and leaving the supernatant with a charge ratio close to the specified global one. The supernatant of the samples remaining, once the precipitate has settled, ranges from clear (at high CR, hence **DOTAP** excess) over slightly blueish (CR = 1 and 0.5, charge equilibrium) to milky (low CR, PE excess). The color indicates differently sized complexes remaining in solution, the complex size increases with decreasing charge ratio.

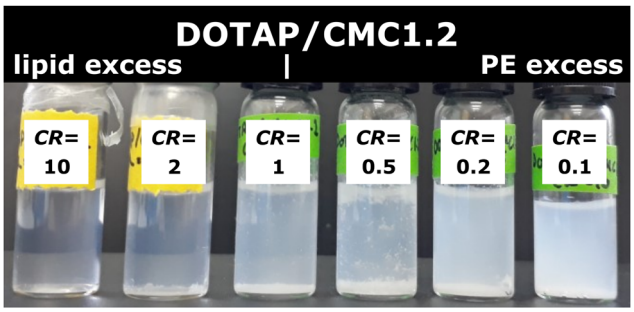

Fig. 2 A series of **DOTAP**/**CMC**1.2 samples at charge ratios ranging from CR = [+]/[−] = 10 to 0.1. Small grainy precipitation can be seen in all samples from CR = 2 to 0.2. The color of the supernatant indicates that the complex size increases with decreasing charge ratio.

Fig. 3 shows cryo-TEM images of three different **DOTAP**/**CMC**1.2 samples at charge ratios CR = 0.5, 0.2, and 0.1 all in the polyelectrolyte excess regime of the phase diagram. The specimens were prepared with the supernatant of the samples only, which had a bluish-to-milky color. As can be seen in Fig. 3, **DOTAP** and **CMC**1.2 form large complexes with a lamellar or multilayered inner structure at all charge ratios; no dependence on the charge ratio is visible in these images. Here it is important to note, that cryo-TEM images show only a projection of the sample, as we are looking at it in transmission mode. Lamellar stacks that are oriented perpendicular to the electron beam show the nice characteristic pattern seen in Fig. 3, while all other orientations show either blurred lamellae or no pattern at all. Hence, areas that do not show the lamellar pattern in the images, do not necessarily indicate lack of order, but most likely show different orientations of the lamellar stacks relative to the electron beam.

Further analysis of the multilayers (analyzed from 5 different images taken from different locations of the grid) yields an average spacing of 5.32 ± 0.07 nm (see ESI† for multilayer spacing analysis and FFT of the images). The dependence of the overall complex size on the charge ratio is not visible in the cryo-TEM images, due to the polydispersity of the complexes and their tendency to form large agglomerates.

In addition to the polyelectrolyte excess regime, we also investigated samples where CR ≥ 1, at lipid excess. Also here, the samples show multilayered complexes. With increasing **DOTAP** excess (higher CR), however, **DOTAP** vesicles can be found coexisting with the mixed complexes, as the available amount of polyelectrolyte is insufficient to sufficiently complex all available **DOTAP** (Fig. S4, ESI†).

While the cryo-TEM images give easily accessible qualitative information about the lamellar nature of the complexes, quantitative and especially statistically relevant information is harder to obtain. Thus, the same samples were also analyzed by small-angle X-ray scattering (SAXS), as shown in Fig. 4. All

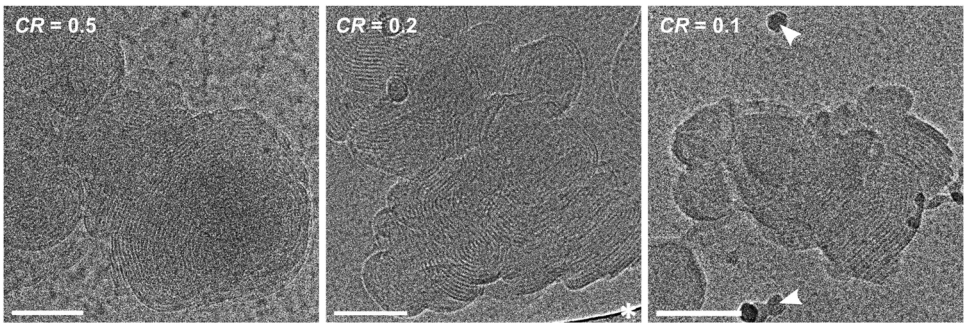

Fig. 3 Cryo-TEM images of 1 mM **DOTAP** mixed with **CMC**1.2 at different charge ratios, all at polyelectrolyte excess. Left: CR = 0.5, middle: CR = 0.2, right: CR = 0.1. All samples form multilayered complexes, with no visible change as function of the charge ratio. A white asterisk indicates a part of the perforated carbon film, dark spots are ice crystals (white arrowheads). Scale bars correspond to 100 nm.

SAXS curves show a clear first-order correlation peak at $q^* \sim 1.2$ nm^{-1}, this peak arises from the inner order of the complexes. In some curves a second-order lamellar peak is also visible, indicating a higher order of the multilayers. For lamellar structures the 1st order peak is expected at q^*, the 2nd order peak at $2{\cdot}q^*$, the 3rd order peak at $3{\cdot}q^*$, and so on. The peaks found here match this pattern and therefore confirm the existence of the ordered lamellar structure we see in the cryo-TEM images. From the position of the 1st order peak, the repeating distance can be calculated *via* $d = 2\pi/q_{max} \sim 5.2$ nm. This value is in good agreement with the layer thickness deduced from the cryo-TEM images. It can be seen that the position of the 1st order peak is unaffected by the CR, so the spacing between the multilayers does not change, as was also found in the cryo-TEM images. This finding seems logical since the spacing of the multilayers should depend mostly on the materials used and not on their mixing ratio.

Fig. 4 right is exemplarily shown in the ESI† as Fig. S6 with errors. It can be seen, that the error bars are smaller than the shown symbols in all cases, and all peaks, including higher order peaks, are significant compared to the error. Thus, errors are omitted for more clarity in other SAXS graphs.

However, some differences in the heights of the peaks can be observed (see normalized Fig. S5 (ESI†) for a better comparison of peak height). At CR = 10, a very high mixing ratio, the peak is very small and also somewhat broader than at the other mixing ratios. Here, there is only very little **CMC**1.2 present in the system, so not as many complexes can be formed, and their layers are less ordered. Whether excess **DOTAP** exists in the system cannot be easily seen from the scattering data. At a slightly lower CR of 2, the 1st order peak is already clearly visible, and the 2nd order peak is just emerging. At CR = 1, the 2nd order peak is clearly visible, but it is most pronounced at CR = 0.5, showing that at this charge ratio, the multilayers have reached their highest ordered state. The CR = 0.5 curve also shows a generally lower intensity than the other ones, which can be explained by the large amount of precipitation, which occurred in this sample. Less material is left in solution, which results in a lower scattering intensity.

When lowering the charge ratio even further to polyelectrolyte excess, it can be seen that the 2nd order peak is disappearing again (CR = 0.2). At CR = 0.1, there is a large excess of polyelectrolyte in the system, which is not participating in the complex formation, but adding to the background scattering.

One might wonder why the highest ordering is achieved at CR = 0.5, at PE excess, and not at the equimolar charge ratio of CR = 1. This can be explained by the degree of deprotonation of the PE, which could be controlled by the pH, but this parameter was already studied elsewhere,[25] and would be

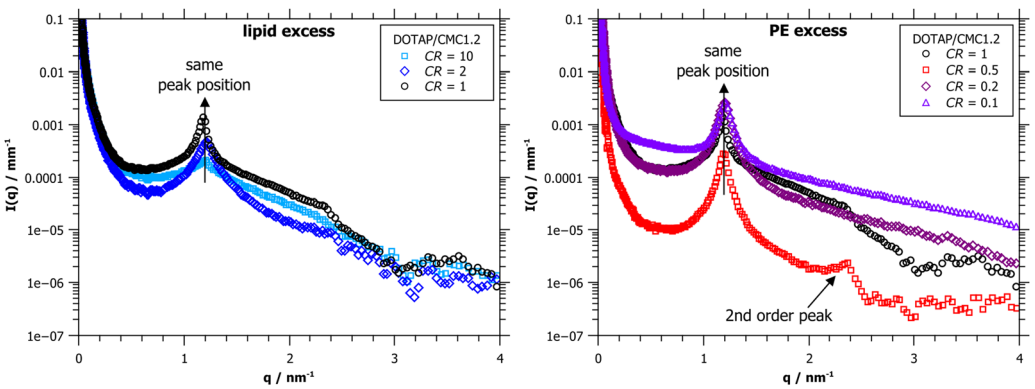

Fig. 4 SAXS data of the series **DOTAP**/**CMC**1.2, *c*(**DOTAP**) = 1 mM, at different CR. Left: CR > 1, right: CR < 1. It can be seen, that the position of the characteristic lamellar peaks remains unchanged by the variation of CR. The 2nd order peak can only be seen in some of the spectra.

beyond the scope of this manuscript. If the polyelectrolyte is not fully deprotonated at the given conditions, the actual charge ratio would be higher than the nominal one, meaning more PE would be needed to reach charge equilibrium. For that reason, experimentally, we find the highest ordering at CR = 0.5 and not CR = 1. This also explains the large amount of precipitate visually observed in the sample at CR = 0.5.

Effect of the polyelectrolyte charge density

Next, we explored the effect of the charge density of the polyelectrolyte. **CMC** is a sugar polymer, where some functional groups are substituted with carboxylates. By varying the degree of substitution (DS) it is possible to change the charge density while maintaining the polyelectrolyte architecture. We used three **CMC**s, all of M_W = 250 kg mol^{-1}, with DS = 0.7, 0.9, and 1.2. As mentioned above, DS is the average number of substituted functional groups per monomer unit, which translates to approximately the same number of charges per nm.

Samples were prepared analogously to the samples described above, mixing the different **CMC** solutions with the **DOTAP** stock solution, this time at a constant charge ratio of CR = 0.5, where the most ordered complexes had been found. Just as before, samples were examined by visual inspection, cryo-TEM, and SAXS.

From the visual appearance of the samples, it becomes obvious, that not the same amount precipitated from all samples (see Fig. S7, ESI†). The amount of precipitate decreases with increasing charge density (DS). In addition, the color of the supernatant changes from colorless to slightly blueish, which indicates an increase in particle size in the supernatant with increasing charge density of the polyelectrolyte.

Cryo-TEM images were taken of the three samples (Fig. 5). All images show large multilayered complexes. No systematic difference in the aggregate size could be determined by cryo-TEM because the aggregates are too large and too polydisperse in size to allow a reliable comparison between the three systems. From the images, it appears that the spacing of the multilayers within the structures does not change with DS. This is expected because the layer thickness depends on the polyelectrolyte backbone and on its flexibility, not on the charge density.

It should be added that all complexes shown in this work were extremely radiation sensitive, allowing only very short exposure times of ~1 s in the low-dose imaging mode, where only ~15 e$^-$ Å^{-2} were used. Higher electron doses resulted in destruction of their structure by electron-beam radiation-damage.[37]

A more quantitative comparison can be obtained by SAXS. In Fig. 6, we note the correlation peak, that arises from the ordered multilayered structure, increasing in intensity with increasing charge density (see normalized data in Fig. S8 for a better comparison of the peak height, ESI†). An increase in the peak area means, that more material exists in this conformation. The narrowing of the peak can be interpreted as a higher order in the system. In addition, the 2nd order peak of lamellar structures cannot be seen in the DS = 0.7 curve, emerging in the DS = 0.9 curve, and is clearly visible at DS = 1.2. It seems that the higher the charge density of the polyelectrolyte, the easier it is for the system to form ordered structures. Hence, the highest ordered systems can be found at the highest charge densities. In Fig. 6, it seems, that the 2nd order peak of the DS = 1.2 curve is shifted towards higher q, compared to the one of DS = 0.9. When looking at the numbers though, this difference is rather small (compare peak positions in Table S1, ESI†). Whether this difference actually reflects a slightly lower lamellar spacing of the DS = 1.2 complexes compared to the lower charge densities (5.33 *vs.* 5.39 nm), cannot be said for certain.

The effects of the nature of the polyelectrolytes

We are also interested in the influence of the polyelectrolyte backbone on the complex formation. Here, we probed four very different polyelectrolytes: **NaPA**, **CMC**, **PSS**, and **DNA**. These four polyelectrolytes differ not only in their flexibility, *i.e.*, the persistence length, l_P (**NaPA** < **CMC** ~ **PSS** < **DNA**), but also in their bulkiness or backbone diameter (**NaPA** < **PSS** < **CMC** < **DNA**), as well as in their charge density (**CMC** < **NaPA** < **PSS** < **DNA**); see also Table 1 for an overview of all the different PE.

When analyzing the visual appearance (Fig. S9, ESI†) of the samples with different polyelectrolytes and **DOTAP**, at the same charge ratio of CR = 0.5, it is clearly seen, that the amount of precipitation decreases with increasing charge density, and also the color of the supernatant strengthens, indicating larger aggregates. This was already observed for the different **CMC**s (0.7–1.2 charges per nm), but this finding can now be

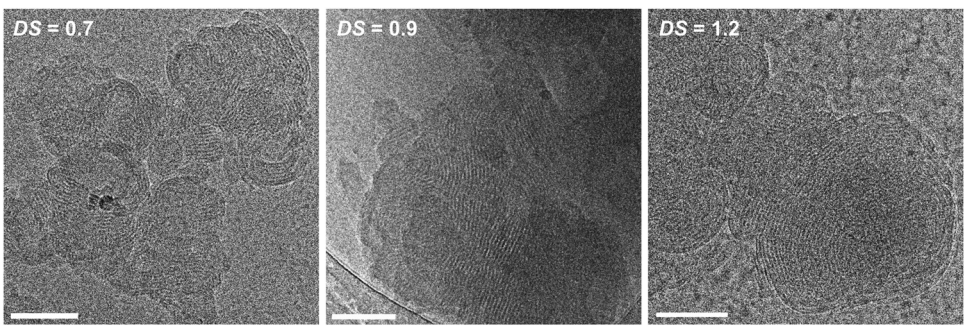

Fig. 5 Cryo-TEM images of 1 mM **DOTAP** mixed with **CMC** of different degrees of substitution (DS), all at CR = 0.5. The three samples form multilayered complexes, with no visible difference between them. Scale bars correspond 100 nm.

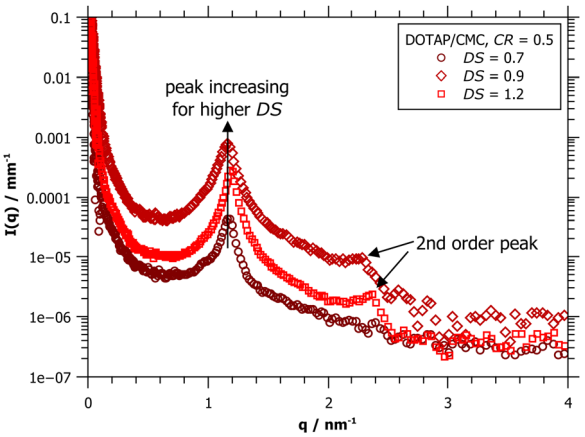

Fig. 6 SAXS data of 1 mM **DOTAP** mixed with **CMC** of different charge densities, DS = 0.7, 0,9 and 1.2, all at CR = 0.5. The 1st and 2nd order peaks both increase with higher charge density, indicating an increased order of the multilayer structures within the aggregates.

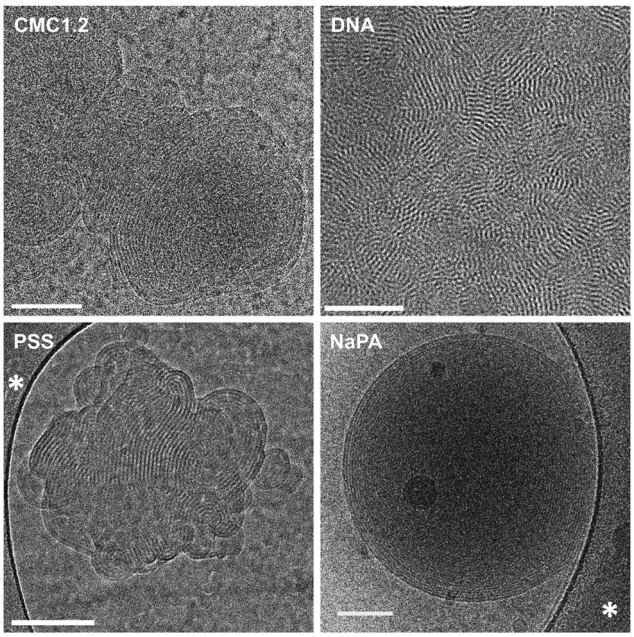

Fig. 7 Cryo-TEM images of 1 mM **DOTAP** mixed with different polyelectrolytes, all at CR = 0.5. All samples form multilayered complexes, but the overall size of the complexes, as well as the order and the spacing of the multilayers depends on the polyelectrolyte. The large dark domains are parts of the perforated carbon film (white asterisk). Scale bars correspond to 100 nm (except for **NaPA**: 50 nm).

generalized for different polyelectrolytes as well. The **DNA** sample (5.9 charges per nm) still shows a very small amount of precipitation, despite having the highest charge density, while the **NaPA** (3.1 charges per nm) and **PSS** (4 charges per nm) samples are completely homogeneous.[38] Due to the double helical structure, **DNA** is also the stiffest polyelectrolyte, which indicates that this is also an important parameter for complex formation. Thus, the charge density directly influences the ability of the polyelectrolyte to form stable complexes with **DOTAP**, but a certain flexibility of the polyelectrolyte chain is also needed.

The cryo-TEM images of Fig. 7, show a range of different structures for different polyelectrolytes. Especially **NaPA** samples form highly ordered, spherical, multilayered complexes. In contrast to the complexes seen previously. These complexes are of very defined round shape and are made of very neatly organized layers. It seems that the high charge density of **NaPA**, together with its very flexible backbone (l_P = 1.3–1.5 nm),[39,40] allow it to organize into these well-formed structures, as it has also been observed before.[25,41] It is interesting to note, that **PSS** with an even higher charge density but slightly lower flexibility (l_P = 10 nm)[38] does not form similarly ordered complexes. The backbones of the two other polyelectrolytes, **CMC** and **DNA**, are also much more rigid than that of **NaPA**, which results in less organized arrangements (l_P(**CMC**) = 6–16 nm; l_P(**DNA**) ~ 40–80 nm).[42,43] The comparison between **DNA** and **CMC** samples shows a slightly higher order for **DNA**, most likely because of the very high charge density. However, the rigid double-helical backbone of **DNA** prevents it from bending into uniform spherical multi-layered aggregates, like **NaPA**.

It also becomes apparent in these images, that the layer thickness of the formed complexes strongly depends on the polyelectrolyte. **NaPA** with the thinnest and most flexible backbone forms very narrow layers, while the double-helical **DNA** shows a much larger spacing.

This difference in layer thickness is confirmed by SAXS measurements (Fig. 8). The characteristic multilayer peak is shifting towards smaller q values with increasing polyelectrolyte diameter, which directly translates to larger repeat distances. The values calculated from the peak positions are: d = 4.6 nm for **PSS**, d = 4.95 nm for the narrow and very flexible **NaPA** molecules, d = 5.33 nm for **CMC**, which is composed of sugar units and therefore already is somewhat bulkier, and the largest spacing with d = 6.03 nm is found for **DNA**, due to its double-helical structure. 2nd order peaks are clearly visible in all of the samples (except for **PSS**, but this is most likely due to

Table 1 Summary of system parameters for the four polymers we studied: the lamellar spacing as deduced from SAXS measurements, width of **DOTAP** double layer subtracted from the lamellar spacing = width of the PE layer within the lamellae, the persistence length of the PE and its charge density

	Spacing (from SAXS) (nm)	Spacing – **DOTAP** double layer (−3.72 nm) (nm)	Persistence length l_P (nm)	Charge density (e^- nm^{-1})
PSS	4.62	0.90	10	4
NaPA	4.95	1.23	1.3	3.1
CMC	5.33	1.61	6–16	0.7–1.2
DNA	6.03	2.31	40–80	5.9

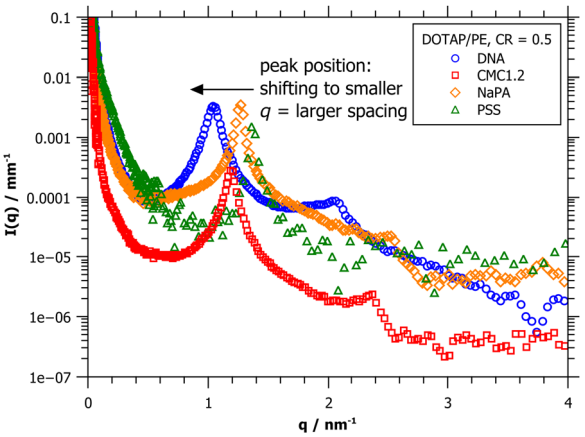

Fig. 8 SAXS data of 1 mM **DOTAP** mixed with different polyelectrolytes, all at CR = 0.5. The peak position is shifting to smaller q, indicating larger spacings, from **PSS** to **NaPA** to **CMC**1.2 to **DNA**.

poor data quality) and appear at $2{\cdot}q^*$, thereby confirming lamellar structures. The overall intensity of the **CMC**-curve is lower, due to the precipitation in that sample.

When comparing the repeat distances of the multilayers as obtained from SAXS with the cryo-TEM images shown in Fig. 7, we are faced with a problem: the layers of the **DOTAP**/**NaPA** complex appear much thinner in the cryo-TEM image than the values obtained from the SAXS peak. This becomes even more clear when comparing the images and numbers with those of **DOTAP**/**PSS** complexes. As mentioned above, the scattering data is better suited for obtaining quantitative results and imaging is prone to artefacts. This is also the case here. Due to the high curvature of the **NaPA** layers in the complex and the transmission mode, the resulting image projection sees an overlay of multiple layers, looking much denser than they are in reality.

Conclusions

We obtained a comprehensive picture of the complexes formed by a positively charged lipid and four very different PEs, and how their nanostructure depends on the different properties of the polyelectrolyte. Although the basic nanostructure of the complexes in these systems is lamellar, their detailed morphology depends strongly on as the mixing ratio, persistence length, charge density, or the PE backbone diameter.

The highest ordered complexes are found at CR = 0.5, below the nominal point of charge equilibrium. This leads to the assumption, that the polyelectrolyte is not fully deprotonated at the studied conditions. The lipid/polyelectrolyte complexes will still achieve their highest ordering at the charge equilibrium, but experimentally we find this point to be at CR = 0.5 and not CR = 1. For transfection, however, usually higher charge ratios at lipid excess are employed.[23] Presumably, the existence of free liposomes boosts the transfection efficiency,[44] and the internal order of the complexes seems to be less important.

The complexes exhibit a higher degree of order the higher the charge density of the polyelectrolyte is. This was shown by

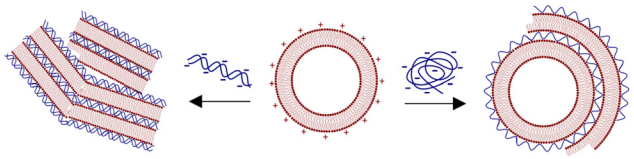

Fig. 9 Sketch of positively charged liposomes interacting with different oppositely charged polyelectrolytes, forming different complex types, depending on the polyelectrolyte properties, such as persistence length, backbone diameter and charge density.

employing **CMC** with different degrees of substitution: the height of the SAXS peak resulting from the lamellar ordering increased with increasing charge density. The very flexible and very highly charged **NaPA** even forms very symmetrical spherical multi-layered complexes, when interacting with **DOTAP**, showing that the interaction, not only depends on the mixing ratio and the charge density but also on the persistence length of the PE. If the polyelectrolyte is very flexible, like **NaPA**, it may bend around the previously existing vesicles and form multi-layered spheres. Stiffer polyelectrolytes break up the spherical shapes of the vesicles and form lamellar stacks that are randomly oriented within one complex. Fig. 9 shows a schematic of this situation.

Finally, the multilayer spacing is influenced by many parameters. By SAXS we found: d(**PSS**) = 4.6 nm < d(**NaPA**) = 4.95 nm < d(**CMC**) = 5.33 nm < d(**DNA**) = 6.03 nm. Naturally, a very bulky backbone like that of the double-helix **DNA** requires more space than the thin sodium polyacrylate. Hence, one could argue, that the backbone diameter of the polyelectrolyte defines the lamellar spacing. The persistence length could also be the dominating parameter since more flexible polymers could fold up more densely on top of the lipid bilayer, and therefore result in smaller lamellar spacings. But since we found the lamellar spacings with **PSS** to be smaller than with **NaPA**, both of these explanations cannot be the only factor here.

When the diameter of the pure lipid bilayer (3.72 nm) is subtracted from the lamellar spacing, it becomes clear, that the remaining space, which must be filled by the polyelectrolyte, is rather narrow (see Table 1). Geometrically it seems unlikely for any polyelectrolyte to be in a coiled or folded formation, independent of its persistence length. Hence, more factors, other than the persistence length must be influencing this situation. Possibly due to the slightly higher charge density of **PSS**, more electrostatic bonds are formed, freeing more Cl^- ions (**DOTAP** counterions), which then enables a denser packing. Maybe other, hard-to-define parameters like hydration of the polyelectrolyte chain are the important parameters here. But on this, we can only speculate. Most likely it is a combination of all parameters mentioned above, that influences the multilayer formation, which means, that the lamellar spacing of lipid/polyelectrolyte complexes remains hard to predict.

Understanding the specific relations between lipids and oppositely charged polyelectrolytes, including the many very sensitive parameters that influence the final aggregate, is essential for the development of finetuned complexes as they are needed for optimized drug and genetic material delivery.

Data availability

All the experimental data, on which our manuscript is based, is available on request.

Conflicts of interest

There are no conflicts to declare.

Acknowledgements

The authors thank the ESRF and T. Narayanan for provision of SAXS beamtime at ID02. M. S. thanks the Minerva Fellowship Programme for funding her postdoctoral project and research work at the Technion in Israel. This work was supported by the Israel Science Foundation, Grant #2302/20 to Y. T. The cryo-TEM work was performed at the Technion Center for Electron Microscopy of Soft Matter.

References

1 J. N. Israelachvili, D. J. Mitchell and B. W. Ninham, *J. Chem. Soc., Faraday Trans. 2*, 1976, **72**, 1525–1568.
2 D. D. Lasic, *Angew. Chem., Int. Ed. Engl.*, 1994, **33**, 1685–1698.
3 L. Sercombe, T. Veerati, F. Moheimani, S. Y. Wu, A. K. Sood and S. Hua, *Front. Pharmacol.*, 2015, **6**(286), 1–13.
4 A. D. Bangham, M. M. Standish and J. C. Watkins, *J. Mol. Biol.*, 1965, **13**, 238–252.
5 M. Bilal and H. M. N. Iqbal, *Cosmetics*, 2020, **7**(24), 1–16.
6 T. M. Taylor, J. Weiss, P. M. Davidson and B. D. Bruce, *Crit. Rev. Food Sci. Nutr.*, 2005, **45**, 587–605.
7 D. D. Lasic, *Trends Biotechnol.*, 1998, **16**, 307–321.
8 E. F. Marques, O. Regev, A. Khan, M. G. Miguel and B. Lindman, *Macromolecules*, 1999, **32**, 6626–6637.
9 B. Biruss and C. Valenta, *J. Pharm. Sci.*, 2007, **96**, 2171–2176.
10 A. Raudino and F. Castelli, *Macromolecules*, 1997, **30**, 2495–2502.
11 P. L. Felgner, T. R. Gadek, M. Holm, R. Roman, H. W. Chan, M. Wenz, J. P. Northrop, G. M. Ringold and M. Danielsen, *Proc. Natl. Acad. Sci. U. S. A.*, 1987, **84**, 7413–7417.
12 M. Brgles, M. Šantak, B. Halassy, D. Forcic and J. Tomašić, *Int. J. Nanomed.*, 2012, **7**, 393–401.
13 N. J. Zuidam, D. Hirsch-Lerner, S. Margulies and Y. Barenholz, *Biochim. Biophys. Acta, Biomembr.*, 1999, **1419**, 207–220.
14 B. Ma, S. Zhang, H. Jiang, B. Zhao and H. Lv, *J. Controlled Release*, 2007, **123**, 184–194.
15 C. R. Safinya, Structures of Lipid-DNA Complexes: Supramolecular Assembly and Gene Delivery, *Curr. Opin. Struct. Biol.*, 2001, **11**, 440–448.
16 S. Golan, B. S. Aytar, J. P. E. Muller, Y. Kondo, D. M. Lynn, N. L. Abbott and Y. Talmon, *Langmuir*, 2011, **27**, 6615–6621.
17 I. Koltover, T. Salditt, J. O. Rädler and C. R. Safinya, *Science*, 1998, **281**, 78–81.
18 S. Even-Chen, R. Cohen and Y. Barenholz, *Chem. Phys. Lipids*, 2012, **165**, 414–423.
19 K. K. Ewert, H. M. Evans, A. Zidovska, N. F. Bouxsein, A. Ahmad and C. R. Safinya, *J. Am. Chem. Soc.*, 2006, **128**, 3998–4006.
20 C. L. Pizzey, C. M. Jewell, M. E. Hays, D. M. Lynn, N. L. Abbott, Y. Kondo, S. Golan and Y. Talmon, *J. Phys. Chem. B*, 2008, **112**, 5849–5857.
21 Y. S. Mel'Nikova, S. M. Mel'Nikov and J. E. Löfroth, *Biophys. Chem.*, 1999, **81**, 125–141.
22 A. Masotti, G. Mossa, C. Cametti, G. Ortaggi, A. Bianco, N. Del Grosso, D. Malizia and C. Esposito, *Colloids Surf., B*, 2009, **68**, 136–144.
23 D. Simberg, D. Danino, Y. Talmon, A. Minsky, M. E. Ferrari, C. J. Wheeler and Y. Barenholz, *J. Biol. Chem.*, 2001, **276**, 47453–47459.
24 S. Golan and Y. Talmon, *Langmuir*, 2012, **28**, 1668–1672.
25 M. Ram-On, Y. Cohen and Y. Talmon, *J. Phys. Chem. B*, 2016, **120**, 5907–5915.
26 L. Chiappisi, S. Prévost, I. Grillo and M. Gradzielski, *Langmuir*, 2014, **30**, 1778–1787.
27 T. Neumann, S. Gajria, N. F. Bouxsein, L. Jeager and M. Tirrell, *J. Am. Chem. Soc.*, 2010, **132**, 7025–7037.
28 U. Lächelt and E. Wagner, *Chem. Rev.*, 2015, **115**, 11043–11078.
29 S. Rappoport, V. Chrysostomou, S. Pispas and Y. Talmon, *Soft Matter*, 2023, **19**, 3688–3699.
30 K. Tanaka and Y. Okahata, *J. Am. Chem. Soc.*, 1996, **118**, 10679–10683.
31 J. R. Bellare, H. T. Davis, L. E. Scriven and Y. Talmon, *J. Electron Microsc. Tech.*, 1988, **10**, 87–111.
32 Y. Talmon, *J. Mol. Liq.*, 2015, **210**, 2–8.
33 Y. Yan, H. Hoffmann, A. Makarsky, W. Richter and Y. Talmon, *J. Phys. Chem. B*, 2007, **111**, 6374–6382.
34 T. Narayanan, M. Sztucki, T. Zinn, J. Kieffer, A. Homs-Puron, J. Gorini, P. Van Vaerenbergh and P. Boesecke, *J. Appl. Crystallogr.*, 2022, **55**, 98–111.
35 J. O. Rädler, I. Koltover, A. Jamieson, T. Salditt and C. R. Safinya, *Langmuir*, 1998, **14**, 4272–4283.
36 S. Golan and Y. Talmon, *Langmuir*, 2012, **28**, 1668–1672.
37 Y. Talmon, *J. Microsc.*, 1982, **125**, 227–237.
38 R. Krishnaswamy, P. Mitra, V. A. Raghunathan and A. K. Sood, *Europhys. Lett.*, 2003, **62**, 357–362.
39 J. Dong, Y. Ozaki and K. Nakashima, *J. Polym. Sci., Part B: Polym. Phys.*, 1997, **35**, 507–515.
40 W. J. Walczak, D. A. Hoagland and S. L. Hsu, *Macromolecules*, 1992, **25**, 7317–7323.
41 S. Golan and Y. Talmon, *Langmuir*, 2012, **28**, 1668–1672.
42 C. W. Hoogendam, A. de Keizer, M. A. Cohen Stuart, B. H. Bijsterbosch, J. A. M. Smit, J. A. P. P. van Dijk, P. M. van der Horst and J. G. Batelaan, *Macromolecules*, 1998, **31**, 6297–6309.
43 Y. Lu, B. Weers and N. C. Stellwagen, *Biopolymers*, 2001, **61**, 261–275.
44 Y. K. Song and D. Liu, *Biochim. Biophys. Acta, Biomembr.*, 1998, **1372**, 141–150.

